Coupled Thermomechanical Analysis of SMA Structures

Chenna Sai Krishna Chaithanya, Animesh Kundu, and Atanu Banerjee

Abstract Of late, shape memory alloys (SMA) are found in a wide variety of applications in the field of aerospace, robotics, biomedical, etc., due to their well-known behaviors called *shape memory effect* and *superelasticity*. To simulate the behavior of these alloys several constitutive models are proposed over the past four decades. To the best of authors' knowledge, in most constitutive models, temperature is considered as an input variable. However, in practice, it evolves as a state variable, depending on applied thermal and mechanical loads and material properties. Moreover, the martensitic transformation processes exhibit endothermic and exothermic effects, significantly affecting temperature and the response. Hence, a fully coupled thermomechanical finite element-based analysis tool is required to simulate the behavior of these materials. The objective of this work is to develop a coupled thermomechanical analysis tool to predict the response of SMA structures under practical thermomechanical loading conditions in ABAQUS. The thermodynamic-based constitutive model, as proposed by Lagoudas and coworker, is implemented in UMAT, a user material subroutine of ABAQUS, to analyze the response of SMA-based components, considering the effect of material level coupling terms, i.e., the latent heat of transformation and thermoelastic heating effects. The results emphasize a significant difference in the transient response of SMA structures while thermal coupling terms are considered, illustrating the importance of the coupled analysis of these materials. Finally, the response of SMA biomedical staple, used for idiopathic scoliosis treatment of the vertebral body, is simulated using the developed FE tool, considering the practical thermomechanical loading conditions.

Keywords Shape memory alloy · Coupled thermomechanical analysis · Material nonlinearity · Latent heat

C. S. K. Chaithanya · A. Kundu (✉) · A. Banerjee
Department of Mechanical Engineering, Indian Institute of Technology Guwahati, Guwahati, India
e-mail: animesh.kundu@iitg.ac.in

K. Jonnalagadda et al. (eds.), *Advances in Structural Integrity*, Lecture Notes in Mechanical Engineering, https://doi.org/10.1007/978-981-16-8724-2_16

1 Introduction

Shape memory alloys (SMA) are active materials with the ability to show large deformations when loaded and recover their shape with the increase in temperature from the deformed shape, known as *shape memory effect (SME)*. In another phenomenon, named *pseudoelasticity (PE)* or *superelasticity (SE)*, it undergoes a large deformation with increment in load and subsequently recovers the same upon unloading. They have high actuation energy densities, which are exploited in a wide variety of applications in the field of aerospace, robotics, biomedical, etc. [1].

The necessity of understanding and modeling the thermomechanical response of SMAs led to the proposal of several constitutive models in the past four decades. In one class of approaches, such as Brinson [2], Tanaka [3], Liang and Rogers [4], the phase evolution is empirically derived from experiments, offering simplicity required for real-time applications; however, they have limited functionality toward modeling under practical thermomechanical loading cases. However, another class of approaches, such as Lagoudas [1], derives the phase evolution based on thermodynamic principles and requires many material parameters. It has been found that for the analyses of practical problems in 2D and 3D, under simultaneous variation of thermomechanical loading, the latter approaches are more suitable.

A vast majority of reported constitutive model considers the phase evolution, derived based on thermodynamic principles, taking temperature as an input variable. However, in reality, temperature is a state variable that depends on applied thermomechanical loads, boundary conditions and internal material properties. Besides, the endothermic and exothermic nature of the phase transformation affects the SMA's temperature and thus renders thermomechanical coupling essential. To effectively predict the response of SMA structures in non-isothermal conditions, a coupled analysis considering the effect of the latent heat and associated heat transfer conditions is necessary. To the best of authors' knowledge, a limited number of studies have been reported on fully coupled thermomechanical analysis by researchers in commercial finite element software.

Yang and Xu [5] incorporated the constitutive model of Seelecke and Muller [6], along with the heat conservation equation to simulate an SMA beam response under a tip force loading in COMSOL Multiphysics FE package. The thermomechanical response of an SMA wire was reported by Alipour et al. [7], under different loading conditions. The one-dimensional constitutive model of Brinson [2] was implemented in ABAQUS UMAT to solve the force and thermal energy conservation equations simultaneously. However, the effect of material level coupling during phase transformation was not considered in this formulation. Sengupta et al. [8] developed a thermomechanically coupled model for SMAs considering large deformation. It was incorporated in FEA package to simulate the response of SMA thin wall tube. Thiebaud et al. [9] implemented the SMA constitutive model of Raniecki and Lexcellent [10] in the COMSOL Multiphysics FE package. The SMA response of a plate in biaxial-tension and in-plane bending is simulated under the isothermal condition and validated using experimental data. Lagoudas et al. [11] proposed a

constitutive model by generalizing the concept of the critical thermodynamic forces for transformation, depending on the applied stress magnitude and the direction of transformation. Smooth hardening function is proposed along with the formation of favored martensitic variants, by applied stress magnitude without specifically accounting for martensitic reorientation. Tabesh et al. [12] reported the influence of latent heat and terms related to thermomechanical coupling on the response of SMA actuator undergoing thermomechanical load, based on the constitutive model of Qidwai and Lagoudas [13]. In 2014, Solomou et al. [14] proposed a 2D beam finite element, following Lagoudas et al. [11], for the coupled thermomechanical analysis of shape memory alloy actuators. First-order shear deformation theory (FSDT) was used, assuming the temperature distribution along the thickness direction as cubic and six-order [15] polynomial.

To design SMA-based components under non-isothermal condition, a thorough apprehension of the effect of the coupling terms, i.e., latent heat, thermoelastic heat and associated heat transfer conditions, is necessary. This article reports a fully coupled thermomechanical analysis of SMA-based structures considering all material level coupling terms. The thermodynamical constitutive model of Boyd and Lagoudas [16], along with numerical implementation scheme, as proposed by Qidwai and Lagoudas [13], is implemented in an incremental-based nonlinear finite element framework. Both the mechanical and thermal equilibrium equations are solved simultaneously, considering latent heat and thermoelastic heat, using Newton–Raphson (NR) iterative scheme. The introduction of heat equation with coupling terms is essential to bring the time scale in the system's transient response. The proposed formulation to predict the response under arbitrary thermomechanical loading is implemented in ABAQUS, through user material subroutine (UMAT).

The organization of the current paper is as follows: First, the constitutive modeling of SMA is discussed briefly in Sect. 2, followed by a coupled finite element formulation. Section 4 illustrates the implementation of the mentioned formulation in the case of the SMA wire and a biomedical staple. It is found that the latent heat, during both forward and backward transformations, impedes the time response of the SMA components. Finally, some concluding remarks are given in Sect. 5.

2 SMA Constitutive Model

In this section, the thermodynamic-based constitutive model is presented for polycrystalline shape memory alloys, as proposed by Boyd and Lagoudas [16]. The Gibbs free energy (G) function is depicted in terms of Cauchy stress (σ_{ij}), temperature (T) and other internal state parameters like martensitic volume fraction (ξ) and transformation strain (ε^t_{ij}). The explicit form of Gibbs free energy is written as

$$G(\sigma_{ij}, T, \xi, \varepsilon^t_{ij}) = -\frac{1}{2\rho}\sigma_{ij}\mathbb{S}_{ijkl}\sigma_{kl} - \frac{1}{\rho}\sigma_{ij}[\alpha_{ij}(T - T_0) + \varepsilon^t_{ij}] + c\left[(T - T_0) - T\ln\left(\frac{T}{T_0}\right)\right] - s_0 T + u_0 + \frac{1}{\rho}f(\xi) \quad (1)$$

Here, T_0 is the reference temperature. The material parameters, $\mathbb{S}_{ijkl}$ depicts the fourth-order effective compliance tensor, α_{ij} signifies the second-order effective thermal expansion tensor, and c denotes the effective specific heat. s_0 and u_0 are the effective specific entropy and effective specific internal energy, respectively, at the reference state. The transformation hardening function is denoted by $f(\xi)$. The effective material properties can be determined by the following expressions:

$$\chi(\xi) = (1 - \xi)\chi_A + \xi\chi_M \quad (2)$$

where $()_M$ and $()_A$ represent SMA properties at pure martensite and austenite phase, respectively. The constitutive relation, to relate stress with strain and temperature using internal material parameters from first and second law of thermodynamics, can be obtained as

$$\varepsilon_{ij} = -\rho\frac{\partial G}{\partial \sigma_{ij}} = \mathbb{S}_{ijkl}\sigma_{ij} + \alpha_{ij}(T - T_0) + \varepsilon^t_{ij} \quad (3)$$

In addition, during phase transformation, the evolution of transformation strain tensor with the formation of martensitic volume fraction, is written as

$$\dot{\varepsilon}^t_{ij} = \Lambda_{ij}\dot{\xi} \quad (4)$$

where Λ_{ij} is the transformation tensor, determining the transformation strain considering the flow direction and is assumed to have the following form:

$$\Lambda_{ij} = \begin{cases} \frac{3}{2}H\frac{\sigma'_{ij}}{\bar{\sigma}} & ; \text{(Forward transformation, } \dot{\xi} > 0) \\ H\frac{\varepsilon^{t-r}_{ij}}{\bar{\varepsilon}^{t-r}} & ; \text{(Backward transformation, } \dot{\xi} < 0) \end{cases} \quad (5)$$

Here, H denotes the maximum uniaxial transformation strain, ε^{t-r}_{ij} is the transformation strain at the reversal of phase transformation. The other terms are expressed as

$$\bar{\sigma} = \sqrt{\frac{3}{2}}\sigma'_{ij}\sigma'_{ij}, \quad \sigma'_{ij} = \sigma_{ij} - \frac{1}{3}(\mathrm{tr}(\sigma_{ij}))\mathrm{I}_{ij}, \quad \bar{\varepsilon}^{t-r}_{ij} = \sqrt{\frac{2}{3}}\varepsilon^{t-r}_{ij}\varepsilon^{t-r}_{ij} \quad (6)$$

This is implemented using *return mapping algorithm* following *elastic predictor-transformation corrector* method in a finite element framework, as given by Qidwai and Lagoudas [13].

3 Coupled Thermomechanical Modeling

The governing differential equations include the stress equilibrium and thermal energy balance equation. The stress equilibrium equation takes the following form:

$$\sigma_{ij,j} + f_i = 0_i \tag{7}$$

The heat energy conservation equation following Lagoudas et al. [11] is written as

$$q_{i,i} + \rho c\dot{T} - q_s - q_{_L} - q_{_t} = 0 \tag{8}$$

and

$$\boldsymbol{q} = \begin{Bmatrix} q_x \\ q_y \\ q_z \end{Bmatrix} = - \begin{bmatrix} k_x & 0 & 0 \\ 0 & k_y & 0 \\ 0 & 0 & k_z \end{bmatrix} \begin{Bmatrix} T_{,x} \\ T_{,y} \\ T_{,z} \end{Bmatrix} = -\boldsymbol{k}\nabla T \tag{9}$$

where $\boldsymbol{q} = \{q_x, q_y, q_z\}$ depicts the heat flux vector (defined in Eq. (9)) related to gradient of temperature by k_x, k_y and k_z, heat conduction coefficients in x, y and z directions, respectively. ρ signifies the density of the material, c is the specific heat and $\dot{T}$ is the time derivative of the material temperature. q_s, $q_{_L}$ and $q_{_t}$ represent the distributed heat sources per unit volume, latent heat absorption or release per unit volume due to phase transformations and the energy release or absorption per unit volume due to the thermoelastic effect, respectively. $q_{_L}$ and $q_{_t}$ are related to stress σ_{ij} and other material parameters, following Lagoudas et al. [11]

$$q_{_L}(\sigma_{ij}, T, \xi) = \left(\pi - \frac{\partial \pi}{\partial T} T\right)\dot{\xi}, \quad q_{_t}(\sigma_{ij}, T, \xi) = -\alpha_{ij}\dot{\sigma}_{ij}T \tag{10}$$

Here, π is the thermodynamic force obtained from Gibbs-free energy. Replacing the thermomechanical coupling terms, one obtains

$$\begin{aligned} q_{_L} + q_{_t} = \Bigg(&\sigma_{ij}\Lambda_{ij} + \frac{1}{2}\sigma_{ij}\Delta\mathbb{S}_{ijkl}\sigma_{ij} - \sigma_{ij}\Delta\alpha_{ij}T_0 \\ &+\rho\Delta c(T - T_0) - \rho\Delta u_0 - \frac{\partial f}{d\xi}\Bigg)\dot{\xi} - \alpha_{ij}\dot{\sigma}_{ij}T \end{aligned} \tag{11}$$

Using standard time discretization procedure [17], Eq. (8) can be written as

$$\rho C\left(\frac{T^{n+1} - T^n}{\Delta t_n}\right) = \theta\psi^{n+1} + (1 - \theta)\psi^n \tag{12}$$

where $\psi = [\boldsymbol{k}(\nabla.(\nabla T)) + q_s + q_{_L} + q_{_t}]$. The superscript n indicates function evaluations at time t_n (similarly for $n+1$) and $\Delta t_n = t_{n+1} - t_n$ is the time step size and $\theta \in [0, 1]$. $q_{_L}$ and $q_{_t}$ (Eq. (10)) are nonlinear terms depending on stress and temperature. After linearization with respect to stress and temperature at nth step, one gets

$$(q_{_L} + q_{_t})^{n+1} = (q_{_L} + q_{_t})^n + \mathcal{X}_{ij}^n \, {}_n\Delta\sigma_{ij} + \mathcal{Y}^n \, {}_n\Delta T \tag{13}$$

where ${}_n\Delta\sigma_{ij}$ and ${}_n\Delta T$ are the increment in Cauchy stress and temperature, respectively, at nth step. $\mathcal{X}_{ij}{}^n$ and $\mathcal{Y}^n$ can be obtained as

$$\mathcal{X}_{ij}^n = \frac{\partial}{\partial \sigma_{ij}}(q_{_L} + q_{_t})^n; \quad \mathcal{Y}^n = \frac{\partial}{\partial T}(q_{_L} + q_{_t})^n$$

Expressing, ${}_n\Delta\varepsilon$ and ${}_n\Delta T$ in terms of increment in nodal displacement ($\Delta \boldsymbol{U}$) and nodal temperature (ΔT) degrees of freedom, respectively, using finite element discretization, the system of equations can be represented as

$$\underbrace{\begin{bmatrix} \boldsymbol{K}_{UU} & \boldsymbol{K}_{UT} \\ \boldsymbol{K}_{TU} & \boldsymbol{K}_{TT} \end{bmatrix}_n}_{\text{Tangent Stiffness Matrix}} \underbrace{\begin{Bmatrix} \Delta \boldsymbol{U} \\ \Delta \boldsymbol{T} \end{Bmatrix}_{n+1}}_{\text{Incremental DOFs}} = \underbrace{\begin{Bmatrix} \Delta \boldsymbol{F}_U \\ \Delta \boldsymbol{F}_T \end{Bmatrix}_{n+1}}_{\text{Residue}} \tag{14}$$

Equation (14) has to be solved iteratively at each time step following Newton–Raphson method (Fig. 1), till the residual of mechanical and thermal load vectors are driven to zero.

4 Result and Discussion

In this section, two representative problems are simulated, demonstrating the capability of the developed FE formulation. Initially, in Sect. 4.1, the thermomechanical response of a pre-strain SMA wire subjected to thermal load at one of its ends is simulated. The same problem has been simulated considering both with and without latent heat and thermoelastic heat terms, to apprehend the effect of coupling terms in the response of SMA wire actuators. In Sect. 4.2, the response of a biomedical staple, used in orthopedic scoliosis treatment, is analyzed to understand the importance of coupling under practical thermomechanical loading. In the discussion, the responses obtained from the developed FE that considers the material level coupling terms (Eq. (10)) are called coupled responses, otherwise referred to as uncoupled responses.

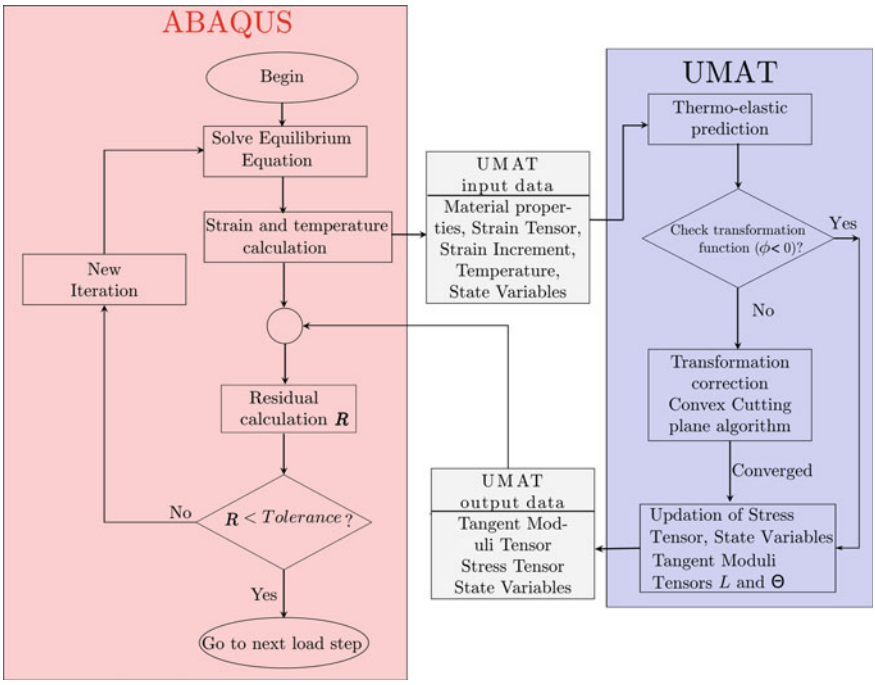

Fig. 1 Flowchart for ABAQUS analysis process for a time step at an integration point of an element

4.1 SMA Wire Heated at One End

An axially pre-strained SMA wire, as shown in Fig. 2a, is initially at the equilibrium state in fully martensitic phase ($\xi = 1$), at the ambient temperature of 310 K. The imparted strain is equal to maximum transformation strain. The wire has a square cross-section of 0.8 mm × 0.8 mm, length of 200 mm and is modeled using a uniform mesh of 20 coupled temperature displacements elements, C3D8T (eight-node thermally coupled brick, trilinear displacement and temperature). The material properties used in this simulation are listed in Table 1. Adiabatic boundary conditions are considered at all faces. Temperature is applied at the free end B, increasing linearly from the environmental temperature of 310 K up to 360 K in 100 s and then remains constant, as shown in Fig. 2a. As the temperature of the heat source is raised, the determination of the wire temperature and end displacement is of primary interest. The simulation is continued until a steady-state condition is reached, that is, the temperature of all nodes is stabilized to a constant value. The results are compared with that presented by Solomou et al. [14] and a good agreement is observed between them.

Figure 2b depicts the evolution of temperature with time under adiabatic condition. As the temperature increases, the endothermic nature of backward transformation

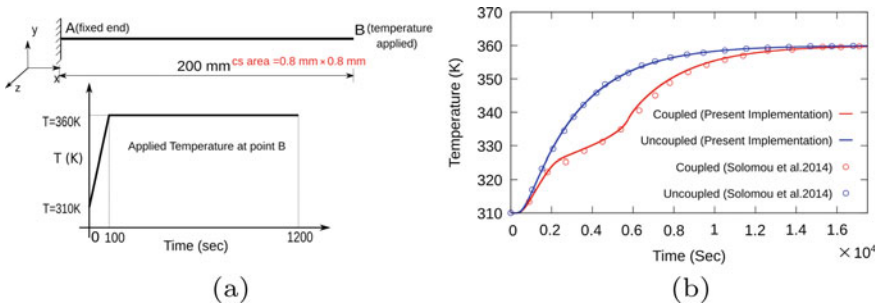

Fig. 2 **a** Schematic diagram of SMA wire fixed at left end A, heated at end B and **b** Evolution of temperature at the fixed end (A)

Table 1 Shape memory alloy material parameters [14]

Material parameter	Symbol	Value
Elastic modulus, Austenite	E^A	66.2 GPa
Elastic modulus, Martensite	E^M	25.6 GPa
Martensite finish temperature	M_f	280 K
Martensite start temperature	M_s	303 K
Austenite start temperature	A_s	325 K
Austenite finish temperature	A_f	338 K
Thermal expansion coefficient, Austenite,	α^A	29×10^{-6}
Thermal expansion coefficient, Martensite,	α^M	29×10^{-6}
Maximum transformation strain,	H	0.031
Stress influence coefficient, Austenite,	C^A	$10.4\,\text{MPaK}^{-1}$
Stress influence coefficient, Martensite,	C^M	$7.3\,\text{MPaK}^{-1}$
Thermal conductivity,	k	18 W/Km
Poisson's ratio	ν	0.33
Density	ρ	$6500\,\text{kgm}^{-3}$

strongly affects the temperature response. There is a change in the slope of temperature response at $t \approx 2000$ s, making the initiation of reverse phase transformation from austenite to martensite. The transformation continues till $t \approx 8000$ s. This is also exhibited through the delayed displacement response (shown in Fig. 3a). Displacement distribution is plotted along the length for different time instants in Fig. 3b. The corresponding temperature and martensite volume fraction distribution along the length are depicted in Fig. 4. However, the temperature distribution is uniform through-thickness of the cross-section. As the heat convection coefficient increases, different portion settles down to different temperature because of heat energy loss to the surroundings and the effect of latent heat diminishes; as a result, the difference in response vanishes.

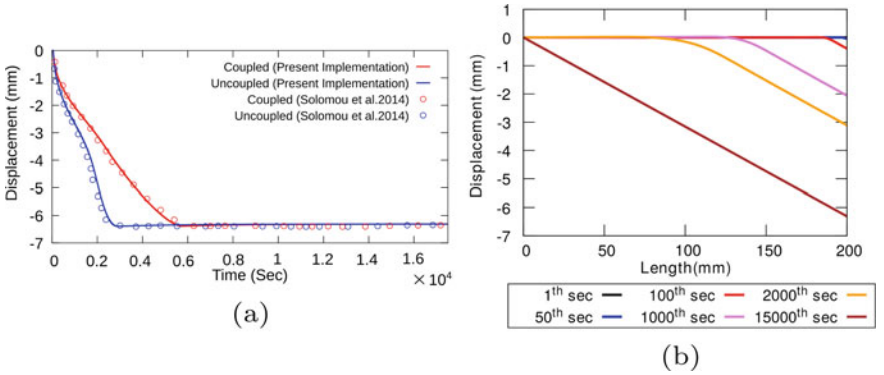

Fig. 3 **a** Difference in displacement response at the free end (B) for uncoupled and coupled analysis, **b** Displacement distribution along the length at different time instants for coupled analysis

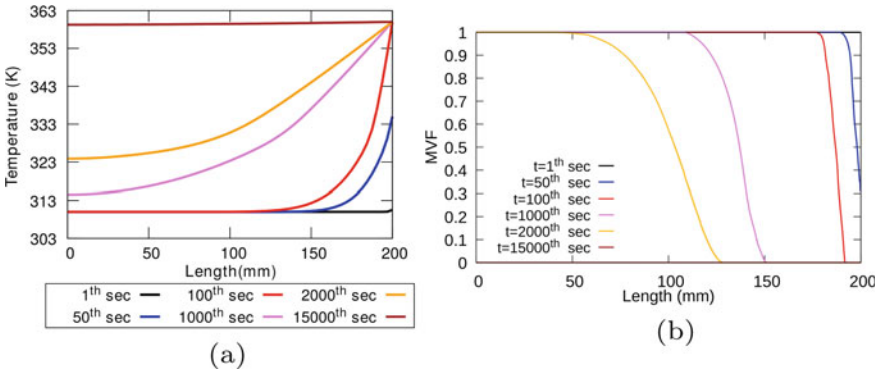

Fig. 4 Predicted distribution of **a** temperature and **b** martensite volume fraction distribution along the length for coupled model at different time instants

4.2 Coupled Thermomechanical Analysis of Biomedical Staple

A NiTi-based biomedical staple is used for hand and foot bone fragments osteotomy fixation and joint arthrodesis, one of the practical applications of SMA. In this problem, the coupled thermomechanical response of a biomedical staple subjected to a practical loading scenario is simulated using the developed FE tool. Following the work of Jaber et al. [18], the staple dimension is shown in Fig. 5, with a rectangular cross-section area of width 2 mm and thickness 2.5 mm. The staple is initially in austenite phase ($\xi = 0$) at a temperature of 288 K. It is loaded with a concentrated force of F = 28 N at each end of the two prongs for 0.9 s and subsequently unloaded in the next 0.1 s. It is then heated to a temperature of 310 K (human body temperature) linearly as shown in applied thermomechanical loading history diagram. The

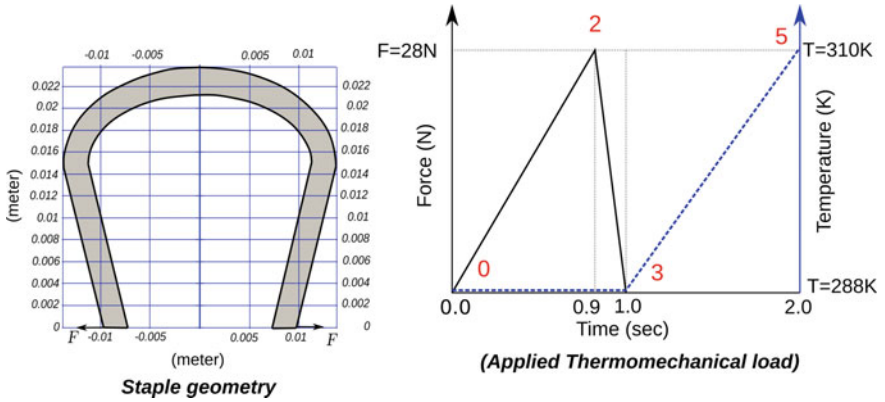

Fig. 5 Schematic of a biomedical staple used for idiopathic scoliosis treatment and applied thermomechanical loading

Table 2 Shape memory alloy material parameters [18]

Material parameter	Symbol	Value
Elastic modulus, Austenite	E^A	70 GPa
Elastic modulus, Martensite	E^M	70 GPa
Martensite finish temperature	M_f	273 K
Martensite start temperature	M_s	283 K
Austenite start temperature	A_s	293 K
Austenite finish temperature	A_f	303 K
Maximum transformation strain,	H	0.06
Stress influence coefficient, Austenite,	C^A	5 MPaK^{-1}
Stress influence coefficient, Martensite,	C^M	5 MPaK^{-1}
Poisson's ratio	ν	0.3
Density	ρ	6500 kgm^{-3}

model is meshed with C3D20T (coupled temperature displacement) elements, to obtain accurate stress distribution and free-end deflection during bending. Adiabatic condition is taken during mechanical loading and during thermal loading temperature boundary condition is used. The material parameters used for the simulation are listed in Table 2. The thermal properties used in this simulation are the same as the ones used in the previous example.

Figure 6 shows the difference in the displacement response for coupled and uncoupled models. As the load increases, initially the response is linear due to elastic loading up to 0.4 s. Further loading leads to starting of forward transformation, resulting in the formation of martensite. This in turn leads to the release of latent heat and thermoelastic heat. As a result, the temperature increases in the zone of higher stresses, which leads to a stiffer model in the presence of coupling terms. On the other hand,

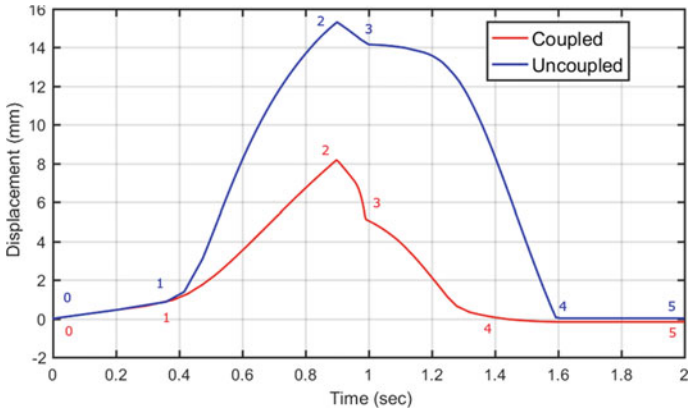

Fig. 6 Displacement response in the direction of F at the point of loading

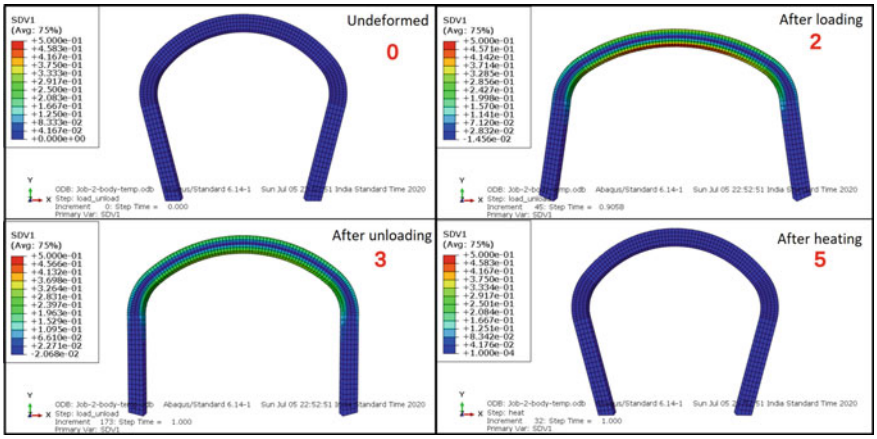

Fig. 7 Martensite volume fraction distribution in the staple for coupled analysis at different time instant

the uncoupled analysis could not capture this phenomenon, as the effects of latent heat and thermoelastic heat are ignored. The corresponding distribution of martensitic volume fraction at different instants is shown in Fig. 7. During unloading from point 2 to point 3 the strain recovery is small as the transformation strain is not recovered. Further, as the temperature increased to 310 K, martensite gets transformed to austenite, bringing the staple back to initial shape.

5 Summary and Conclusion

In this work, a thermomechanically coupled formulation for SMA structures is developed and implemented in a nonlinear finite element framework. The effects of the coupling terms, i.e., latent heat of transformation and thermoelastic heat due to phase transformation, are explored in this formulation. Consideration of mechanical loading applied heat source and boundary conditions significantly alters the performance of the system. To effectively predict the response of SMA-based components, the effect of latent heat is essential to capture the effect of the exothermic or endothermic nature of transformation, especially during phase transformation. Finally, the developed FE is used to find the response of a biomedical staple under practical thermomechanical loading cases. It is found that the coupled analysis is required to effectively predict the thermomechanical response, which cannot be captured using uncoupled analysis. This formulation can be extended for other 2D and 3D applications, such as SMA stents, origami structures, considering geometric nonlinearity, which will be explored in the future.

Acknowledgements The authors thank the support from the Department of Mechanical Engineering, IIT Guwahati and MHRD (Govt of India) for providing necessary facilities and funding. The projects SR/FTP/ETA-0124/2011 and BT/255/NE/TBP/2011, funded by the Department of Science and Technology (DST) and the Department of Biotechnology (DBT), Govt. of India, respectively, are also gratefully acknowledged.

References

1. Lagoudas DC (2008) Shape memory alloys, modelling and engineering applications. Springer, New York
2. Brinson LC (1993) One-dimensional constitutive behavior of shape memory alloys: thermomechanical derivation with non-constant material functions and redefined martensite internal variable. J Intell Mater Syst Struct 4:229–242
3. Tanaka K (1986) A thermomechanical sketch of shape memory effect; one dimensional tensile behavior. Int J Numer Methods Eng 18:251–263
4. Liang C, Rogers CA (1990) One-dimensional thermomechanical constitutive relations for shape memory materials. J Intell Mater Syst Struct 2:207–234
5. Yang SB, Xu M (2011) Finite element analysis of 2d SMA beam bending. Acta Mech Sin 27(5):738
6. Seelecke S, Muller I (2004) Shape memory alloy actuators in smart structures: modeling and simulation. Appl Mech Rev 57(1):23–46
7. Alipour A, Kadkhodaei M, Ghaei A (2015) Finite element simulation of shape memory alloy wires using a user material subroutine: parametric study on heating rate, conductivity, and heat convection. J Intell Mater Syst Struct 26(5):554–572
8. Sengupta A, Papadopoulos P, Kueck A, Pelton AR (2011) On phase transformation models for thermo-mechanically coupled response of nitinol. Comput Mech 48(2):213–227
9. Thiebaud F, Collet M, Foltete E, Lexcellent C (2007) Implementation of a multi-axial pseudoelastic model to predict the dynamic behavior of shape memory alloys. Smart Mater Struct 16(4):935
10. Raniecki B, Lexcellent C (1998) Thermodynamics of isotropic pseudoelasticity in shape memory alloys. Eur J Mech-A/Solids 17(2):185–205

11. Lagoudas D, Hartl D, Chemisky Y, Machado L, Popov P (2012) Constitutive model for the numerical analysis of phase transformation in polycrystalline shape memory alloys. Int J Plast 32:155–183
12. Tabesh M, Lester B, Hartl D, Lagoudas D (2012) Influence of the latent heat of transformation and thermomechanical coupling on the performance of shape memory alloy actuators. In: Smart materials, adaptive structures and intelligent systems, vol 45103, pp 237–248. American Society of Mechanical Engineers
13. Qidwai M, Lagoudas D (2000) Numerical implementation of a shape memory alloy thermomechanical constitutive model using return mapping algorithms. Int J Numer Methods Eng 47:1123–1168
14. Solomou AG, Machairas TT, Saravanos DA (2014) A coupled thermomechanical beam finite element for the simulation of shape memory alloy actuators. J Intell Mater Syst Struct 25(7):890–907
15. Solomou AG, Machairas TT, Saravanos DA, Hartl DJ, Lagoudas DC (2016) A coupled layered thermomechanical shape memory alloy beam element with enhanced higher order temperature field approximations. J Intell Mater Syst Struct 27(17):2359–2384
16. Boyd J, Lagoudas DC (1996) A thermodynamical constitutive model for shape memory materials. Int J Plast 12:805–842
17. Crank J, Nicolson P (1947) A practical method for numerical evaluation of solutions of partial differential equations of the heat-conduction type. In: Mathematical proceedings of the Cambridge philosophical society, vol 43, pp 50–67. Cambridge University Press
18. Jaber MB, Smaoui H, Terriault P (2008) Finite element analysis of a shape memory alloy three-dimensional beam based on a finite strain description. Smart Mater Struct 17(4):045005